Author Manuscript

Author Manuscript

Author Manuscript

Author Manuscript

HHS Public Access

Author manuscript

Clin Cancer Res. Author manuscript; available in PMC 2024 February 15.

Published in final edited form as:

Clin Cancer Res. 2021 February 01; 27(3): 877–888. doi:10.1158/1078-0432.CCR-20-1985.

NRF2 activation promotes aggressive lung cancer and associates with poor clinical outcomes

Anju Singh[1,†], **Anneleen Daemen**[2,†,‡,*], **Dorothee Nickles**[2,†,*], **Sang-Min Jeon**[3,4,†], **Oded Foreman**[5], **Kuladeep Sudini**[1], **Florian Gnad**[2,‡], **Stephane Lajoie**[1], **Naina Gour**[1], **Wayne Mitzner**[1], **Samit Chatterjee**[1], **Eun-Ji Choi**[4], **Buvana Ravishankar**[6,‡], **Amy Rappaport**[7,‡], **Namrata Patil**[8], **Mark McCleland**[8], **Leisa Johnson**[7,‡], **George Acquaah-Mensah**[9], **Edward Gabrielson**[10], **Shyam Biswal**[1,*], **Georgia Hatzivassiliou**[3,^]

[1]Department of Environmental Health Science and Engineering, Johns Hopkins University School of Public Health, Baltimore, MD 210205, USA.

[2]Oncology Bioinformatics, Genentech Inc., South San Francisco, CA 94080, USA.

[3]Translational Oncology, Genentech Inc., South San Francisco, CA 94080, USA.

[4]College of Pharmacy and Research Institute of Pharmaceutical Science and Technology, Ajou University, Suwon, Gyeonggi-do, 16499, Republic of Korea.

[5]Pathology, Genentech Inc., South San Francisco, CA 94080, USA.

[6]Cancer Immunology, Genentech Inc., South San Francisco, CA 94080, USA.

[7]Discovery Oncology, Genentech Inc., South San Francisco, CA 94080, USA.

[8]Oncology Biomarker Development, Genentech Inc., South San Francisco, CA 94080, USA.

[9]Department of Pharmaceutical Sciences, Massachusetts College of Pharmacy and Health Sciences, Worcester, MA 01608, USA.

[10]Department of Pathology and Oncology, School of Medicine, Johns Hopkins University, Baltimore, MD 21231, USA.

Abstract

Purpose: Stabilization of the transcription factor NRF2 through genomic alterations in *KEAP1* and *NFE2L2* occurs in a quarter of lung adenocarcinoma (LUAD) and a third of lung squamous (LUSC) patients. In LUAD, *KEAP1* loss often co-occurs with *STK11* loss and *KRAS* activating

[*]**Corresponding authors**: Anneleen Daemen, Translational Medicine, ORIC Pharmaceuticals, South San Francisco, CA 94080, USA, anneleen.daemen@gmail.com, phone: 650 388 5608; Dorothee Nickles, Oncology Bioinformatics, Genentech Inc., South San Francisco, CA 94080, USA, nicklesd@gene.com, phone: 650 467 8396; Shyam Biswal, Department of Environmental Health Science and Engineering, Johns Hopkins University School of Public Health, Baltimore, MD 210205, USA, sbiswal@jhu.edu, phone: 410 502 1944.

[‡]Current address: Oric Pharmaceuticals (AD), Roche (FG), RAPT Therapeutics (BR), Gritstone Oncology (AR) and 4D Molecular Therapeutics (LJ).

[†]These authors contributed equally to this work.

[^]In memoriam: Georgia was an exceptionally dedicated scientist who profoundly shaped this work and cancer research in general.

Conflict of interest: Authors with a Genentech affiliation may hold company shares. S.B and A.S hold patent number 8216777 titled "Compositions and methods for the treatment or prevention of chemoresistant neoplasia" dated July 10, 2012.

Author Manuscript Author Manuscript Author Manuscript Author Manuscript

alterations. Despite its prevalence, the impact of NRF activation on tumor progression and patient outcomes is not fully defined.

Experimental Design: We model NRF2 activation, *STK11* loss and *KRAS* activation *in vivo* using novel genetically engineered mouse models. Further, we derive a NRF2 activation signature from human non-small cell lung tumors that we use to dissect how these genomic events impact outcomes and immune contexture of participants in the OAK and IMpower131 immunotherapy trials.

Results: Our *in vivo* data reveal roles for NRF2 activation in (i) promoting rapid-onset, multi-focal intra-bronchiolar carcinomas, leading to lethal pulmonary dysfunction, and (ii) decreasing elevated redox stress in *KRAS*-mutant, *STK11*-null tumors. In patients with non-squamous tumors, the NRF2 signature is negatively prognostic independently of *STK11* loss. LUSC patients with low NRF2 signature survive longer when receiving anti-PD-L1 treatment.

Conclusions: Our *in vivo* modeling establishes NRF2 activation as a critical oncogenic driver, cooperating with *STK11* loss and *KRAS* activation to promote aggressive LUAD. In patients, oncogenic events alter the tumor immune contexture, possibly impacting treatment responses. Importantly, patients with NRF2 activated non-squamous or squamous tumors have poor prognosis and show limited response to anti-PD-L1 treatment.

Translational Relevance

Using a functional gene expression signature, we show that NRF2 activation impacts phenotype, prognosis and treatment responses of non-small lung cancer (NSCLC) of both non-squamous and squamous histology. These data suggest that NRF2 activation status should be considered as diagnostic tool to improve treatment efficacy across NSCLC.

Keywords

Non-small cell lung cancer; NRF2; immunotherapy; predictive biomarker; genetically engineered mouse model

Introduction

Non-small-cell lung cancer (NSCLC) is a heterogeneous disease, comprised of distinct histologic and genomic subtypes, each exhibiting unique biology, immune profiles and clinical behavior (1). Genomic alterations in the *KEAP1* and *NFE2L2 (NRF2)* loci are frequent events in NSCLC, and lead to the constitutive stabilization of the transcription factor NRF2, a master regulator of antioxidant defenses, whose protein levels are tightly controlled through proteasome-mediated degradation, mainly by the E3 ubiquitin ligase complex of KEAP1-CUL3-RBX1 (2–5). In lung adenocarcinoma (LUAD), NRF2 activation is the third most frequent genomic event (25%), primarily occurring via *KEAP1* loss-of-function mutations (3,4,6,7). Yet, NRF2 activated tumors occur across LUAD subsets traditionally defined by other oncogenic events such as *KRAS* alterations and *STK11* loss (7,8), and LUAD clinical trial datasets analyzed thus far lack the sample size needed to dissect the impact of NRF2 activation on patient responses (9). We set out to shed more light

Author Manuscript Author Manuscript Author Manuscript Author Manuscript

on the contribution of *KEAP1* loss and NRF2 activation to LUAD development, phenotype, immune contexture and clinical responses.

Genetically engineered mouse models (GEMMs) have so far corroborated a role for *Keap1* loss and/or *Nrf2* activity in promoting and accelerating $Kras^{G12D}$ driven lung tumorigenesis (10–12). Given that in human tumors *KEAP1* loss often co-occurs with loss of the tumor suppressor *STK11* in addition to mutational activation of *KRAS*, GEMMs modeling all three genetic events would be a valuable approach for modeling human disease *in vivo* and for dissecting the contribution of each event in LUAD initiation and phenotype. While a recent study attempted to address this need, the low number of animals used, combined with the challenge of combined targeting across multiple loci, precluded definitive conclusions (12). In the current study, we have taken a multi-pronged and rigorous approach using *in vitro* and *in vivo* preclinical models as well as two large phase III clinical trial cohorts to define the impact of NRF2 activation and its co-operativity with *STK11* loss and *KRAS* activation on lung cancer development and response to chemotherapy and immunotherapy regimens. Our work establishes NRF2 activation as a critical oncogenic driver, cooperating with *STK11* loss and *KRAS* activation to promote aggressive LUAD, with a transcriptional NRF2 activation signature being a potentially important diagnostic tool for evaluating prognostic and therapeutic patient outcomes in human lung cancer.

Materials and Methods

$Kras^{LSL\text{-}G12D}$ (strain number 01XJ6) (39) and $Stk11^{fl/fl}$ (strain number 01XN2) (40) were bred with $Keap1^{fl/fl}$ mice (41) to generate compound mutant mice in our facility. All experimental mice were maintained in mixed genetic background (Stk11- FVB;129S6, Kras - C57B6, Keap1- C57B6). Total glutathione levels, lipid peroxidation levels and 4-HNE were measured as described previously (42–44). Lung physiology metrics were measured as described in (45,46). The method for estimating lung tumor burden was adapted from Krupnick et al (47,48). ROS levels were measured as described previously (49). All experimental protocols conducted on the mice were performed in accordance with National Institutes of Health guidelines and were approved by the Johns Hopkins University Animal Care and Use Committee.

Gene expression profiling of cell line HCC515 and derivatives was performed using Human Genome U133 plus 2.0 arrays (Affymetrix), and of murine tumors using Mouse Gene 2.0 ST arrays (Affymetrix). TCGA RNA-sequencing, Affymetrix SNP6 copy number, and whole exome-sequencing data for 439 lung adenocarcinoma (LUAD) (7) and 306 lung squamous cell carcinoma (LUSC) (24) tumors are from the National Cancer Institute Genomic Data Commons (https://gdc.cancer.gov). We focused on any alteration in *KRAS*, *STK11*, *KEAP1* and *NRF2* (*NFE2L2*) for LUAD, and *TP53*, *KEAP1* and *NRF2* for LUSC, and additionally incorporated amplification of *NRF2*. Alterations in *KEAP1* and *NRF2* were combined, referred to as *KEAP1/NRF2*. For participants of the OAK and IMpower131 trials, genomic alterations were assessed using the FoundationOne® panel, and whole transcriptome profiles were generated using TruSeq RNA Access technology (Illumina®). Details of the PD-L1 immunohistochemistry (IHC) assessment is described in (25). All patients included in this study provided signed informed consent, and clinical trials were conducted in full

Author Manuscript Author Manuscript Author Manuscript Author Manuscript

accordance with the guidelines for Good Clinical Practice and the Declaration of Helsinki. All raw *in vitro* and *in vivo* microarray data are available on the Gene Expression Omnibus (GEO) under accession numbers GSE133714 and GSE133715.

Voom+limma in R was used for differential gene expression analysis, followed by KEGG pathway enrichment analysis. Camera was used for GSEA of the murine lungs by genotype. The Cox proportional hazards model was used for survival analysis. Linear or nested models were fit to assess the relationship between signature/mutation status, PD-L1 protein expression, and/or response. To test (in)dependence of different model terms, likelihood ratio test p values were calculated using ANOVA on nested models. Differences between multiple groups or genotypes was assessed with ANOVA, followed by Dunnett's multiple comparison test, Kruskall-Wallis followed by Dunn's multiple comparison test, or Wilcoxon rank sum test followed by Bonferoni multiple testing correction as stated. Significance was assumed at $p < 0.05$. We refer to supplementary Materials & Methods for more details.

Results

Keap1 inactivation synergizes with Stk11 loss to promote early and diffuse tumor formation, impaired lung function and mortality in Kras-driven lung cancer mouse models in vivo

To characterize the impact of combined loss of *Keap1* and *Stk11* in the context of a $Kras^{G12D}$ activating mutation *in vivo*, we crossed $Keap1^{fl/fl}$ mice to $Kras^{LSL\text{-}G12D}$ mice and $Stk11^{fl/fl}$ mice followed by intra-tracheal administration of adenovirus encoding CMV-Cre-recombinase to delete exons 2–3 of *Keap1* and exons 3–6 of *Stk11* in the mouse lungs (13–16). The following genotypes were generated: (a) $Kras^{LSL\text{-}G12D}$, (b) $Keap1^{fl/fl}Kras^{LSL\text{-}G12D}$, (c) $Stk11^{fl/fl}Kras^{LSL\text{-}G12D}$, (d) $Keap1^{fl/fl}Stk11^{fl/fl}Kras^{LSL\text{-}G12D}$. Real-time PCR (Q-PCR) confirmed reduced expression of *Keap1* and *Stk11* in lungs with the respective genotypes (Fig. S1A). The four described genotypes of our novel GEMMs exhibited striking differences in overall survival (OS), most strikingly a reduced median OS to only 59 days in mice with combined loss of *Keap1* and *Stk11* that became progressively moribund with severe respiratory distress (Fig. 1A).

Transcriptional characterization of the murine lungs further confirmed robust induction of Nrf2 upon *Keap1* deletion. While *Stk11* loss impacted the expression of 19 genes consistently in the absence or presence of concurrent *Keap1* loss, loss of *Keap1* resulted in 304 up- and 147 down-regulated genes, irrespectively of *Stk11* status (>2 fold expression change, adjusted $p < 0.05$; Fig. 1B, Table S1). $Keap1^{fl/fl}Stk11^{fl/fl}Kras^{LSL}$ lungs were uniquely characterized by 59 higher and 169 lower expressed genes compared to all other genotypes, implying synergistic transcriptional implications from co-occurring *Stk11* and *Keap1* loss. Gene set enrichment analysis (GSEA) comparing *Keap1* deficient ($Keap1^{fl/fl}$) to wild-type ($Keap1^{+/+}$) tumor bearing murine lung samples showed induction of glutathione, xenobiotics, pentose phosphate pathway and arachidonic acid metabolism genes in $Keap1^{fl/fl}$-murine lung samples (Fig. S1B, Table S1).

To evaluate tumor burden and identify a cause for the animals' morbidity and short lifespan, we evaluated lung density, function and histology. Direct measurement of tumor burden

Author Manuscript Author Manuscript Author Manuscript Author Manuscript

by micro-computed tomography (CT) was hindered by the diffuse and widely dispersed growth of neoplastic lesions in *Keap1*$^{fl/fl}$*Stk11*$^{fl/fl}$*Kras*$^{LSL\text{-}G12D}$ animals; thus, we assessed lung density as a surrogate measurement of transformed lung tissue across genotypes. The *Keap1*$^{fl/fl}$*Stk11*$^{fl/fl}$*Kras*$^{LSL\text{-}G12D}$ genotype displayed high lung density as early as 4 weeks post-viral infection (pvi) and maintained it at 6 and 8–9 weeks when they succumbed. By comparison, *Stk11*$^{fl/fl}$*Kras*$^{LSL\text{-}G12D}$ lungs showed a lower lung density at 4 weeks, progressively increasing at 6 and 8–9 weeks while *Keap1*$^{fl/fl}$*Kras*$^{LSL\text{-}G12D}$ lungs reached high density at 8–9 weeks. *Kras*$^{LSL\text{-}G12D}$ mice were analyzed only at 8–9 weeks pvi at which timepoint they displayed the lowest lung density across all genotypes, consistent with their more indolent disease course (Fig. 1C–D, Fig. S1C).

By 6–8 weeks pvi, *Keap1*$^{fl/fl}$*Stk11*$^{fl/fl}$*Kras*$^{LSL\text{-}G12D}$ mice were already demonstrating severe respiratory distress. Based on three key functional pulmonary readouts: (i) carbon monoxide diffusion (DF_{CO}); (ii) functional residual capacity (FRC); and (iii) baseline respiratory resistance (Rrs), the *Keap1*$^{fl/fl}$*Stk11*$^{fl/fl}$*Kras*$^{LSL\text{-}G12D}$ mice exhibited maximal lung dysfunction compared to the other genotypes (Fig. 1E–F). These data, combined with the severe respiratory distress and labored breathing in the triple mutant mice, indicated that lung failure, associated with inspiratory muscle fatigue, contributed to the reduced survival of this group.

Histological evaluation of mouse lungs at 7 weeks pvi identified significant differences in both the number and distribution of tumor nodules in *Stk11*$^{fl/fl}$*Kras*$^{LSL\text{-}G12D}$ lungs with versus without *Keap1* loss. In *Keap1*$^{fl/fl}$*Stk11*$^{fl/fl}$*Kras*$^{LSL\text{-}G12D}$ animals, tumors affected all lung lobes and occurred throughout the lung parenchyma from the airways to the pleura (Fig. 1G, Fig. S1D). These lungs contained dozens of distinct foci ranging from atypical adenomatous hyperplasia (AAH) to poorly differentiated adenocarcinomas containing dysplastic cells with abnormal mitotic figures. In contrast, lobes of *Stk11*$^{fl/fl}$*Kras*$^{LSL\text{-}G12D}$ animals contained large, but fewer tumors that appeared to be radiating from the airways into the adjacent parenchyma. Furthermore, such tumors were often surrounded by pools of mucin admixed with necrotic debris. Overall, these data point towards a tumor-promoting effect of *Keap1* loss in the context of *Stk11* loss and *Kras*^{G12D} activation, facilitating earlier onset and multi-focal tumor initiation compared to *Stk11* loss alone.

Keap1$^{fl/fl}$Stk11$^{fl/fl}$Kras$^{LSL\text{-}G12D}$ mice display tumor growth within airways, severe airway obstruction, and mucinous differentiation linked to Stk11 loss

To gain a better understanding of the impact of *Keap1* and *Stk11* loss on lung cancer histology, we performed a more detailed evaluation of lungs at 6–12 weeks pvi. At this early timepoint, one- to two-third of *Stk11*$^{fl/fl}$*Kras*^{LSL} and *Keap1*$^{fl/fl}$*Stk11*$^{fl/fl}$*Kras*$^{LSL\text{-}G12D}$ mutant lungs bore adenomas and adenocarcinomas. Furthermore, for both genotypes lungs developed AAH and both mucinous as well as non-mucinous bronchiolar epithelial hyperplasia (BEH). *Kras*$^{LSL\text{-}G12D}$ and *Keap1*$^{fl/fl}$*Kras*$^{LSL\text{-}G12D}$ lungs developed carcinomas only at later timepoints, 12–24 weeks pvi (Fig. 2A, Fig. S1E, Table 1). Unique among triple mutant lungs was the presence of intra-bronchiolar papillary carcinomas, sometimes completely obstructing the airways (Fig. 2A, green crosses). The combination of these

Author Manuscript Author Manuscript Author Manuscript Author Manuscript

features, absent from the other three genotypes, likely explains the respiratory distress and early-onset mortality in triple mutant mice.

Interestingly, all adenomas and adenocarcinomas in *Stk11*$^{fl/fl}$*Kras*$^{LSL\text{-}G12D}$ mice showed evidence of mucinous differentiation; this phenomenon was only apparent in 43% of carcinomas in *Keap1*$^{fl/fl}$*Stk11*$^{fl/fl}$*Kras*$^{LSL\text{-}G12D}$ lungs (Fig. 2A, Fig. S1F, Table 1). Staining for mucins using Alcian Blue/PAS at 6–7 weeks pvi confirmed mucin production in *Stk11*$^{fl/fl}$*Kras*$^{LSL\text{-}G12D}$ and *Keap1*$^{fl/fl}$*Stk11*$^{fl/fl}$*Kras*$^{LSL\text{-}G12D}$ lungs; in contrast, *Kras*$^{LSL\text{-}G12D}$ and *Keap1*$^{fl/fl}$*Kras*$^{LSL\text{-}G12D}$ lungs displayed only non-mucinous AAH (Fig. 2B). The association of a mucinous differentiation phenotype with *Stk11* loss was further supported by a 6–10-fold increase in the mRNA expression of the canonical mucinous marker genes *Muc5b* and *Agr2* in *Stk11*$^{fl/fl}$ versus *Stk11* wild-type lungs ($p = 0.0002$ and 0.002, respectively; Fig. 2C, Table S1). Consistent with the mouse data, a significantly higher expression of the mucinous markers *MUC5AC*, *MUC5B* and *AGR2* was present in *STK11*-mutant human tumors from TCGA LUAD (7), independent of *KEAP1/NRF2* status (Fig. 2D). Mucinous differentiation is often associated with deleterious mutations and/or decreased expression of the NKX2 homeobox 1 (NKX2–1 or TTF1) protein, a lineage-specific transcription factor that negatively regulates mucinous marker expression (17). Yet, our mouse lung adenocarcinomas stained positive for TTF1/NKX2–1, including the areas of mucinous differentiation and independently of genotype (Fig. S1E–F). By contrast, there was a modest decrease in *Nkx2–1* expression in *Keap1*$^{fl/fl}$*Stk11*$^{fl/fl}$*Kras*$^{LSL\text{-}G12D}$ lungs at the mRNA level (1.5-fold, $p = 0.018$), but we found no evidence of a downregulation in *Stk11*$^{fl/fl}$*Kras*$^{LSL\text{-}G12D}$ lungs (Fig. 2C, Table S1). Consistent with the mouse phenotypes, *STK11* status had no impact on *NKX2–1* levels in the human LUAD TCGA dataset, whereas *NKX2–1* mRNA levels were ~2-fold lower among *KEAP1/NRF2*-mutant tumors (Fig. 2E). An additional characteristic of the *Stk11*$^{fl/fl}$*Kras*$^{LSL\text{-}G12D}$ genotype was the presence of squamous carcinomas in 40% of lungs at 12–19 weeks psi, consistent with previous reports (18). Finally, quantification of Ki67-positive nuclei across tumor histotypes revealed an overall higher proliferation rate among *Keap1*$^{fl/fl}$*Stk11*$^{fl/fl}$*Kras*$^{LSL\text{-}G12D}$ compared to *Stk11*$^{fl/fl}$*Kras*$^{LSL\text{-}G12D}$ tumors of any histology (Fig. S1G). Differences by genotype per histology did not reach significance due to the small sample size.

In summary, our GEMMs and TCGA analyses provide additional insights into the impact of *Keap1* versus *Stk11* loss on LUAD differentiation and progression, revealing phenotypes specific to *Stk11* loss (namely a high frequency of mucinous adenocarcinomas arising independently of changes in *Nkx2–1* mRNA levels) and those exacerbated by combined *Keap1* loss (early onset tumorigenesis, high proliferation rates, presence of intra-bronchiolar carcinomas and association with moderately lower *Nkx2–1* mRNA expression). The cross-species concordance suggests that our mouse LUAD model faithfully recapitulates human LUAD phenotypes.

Keap1 loss counteracts the increase in redox stress induced upon Stk11 inactivation in a Kras-driven lung cancer mouse model in vivo

We have previously shown that *STK11* loss limits the flexibility of tumor cells to overcome bioenergetic and redox stress, due to defective AMPK activation and decreased NADPH

Author Manuscript Author Manuscript Author Manuscript Author Manuscript

levels (19). Hence, we evaluated the impact of *Keap1* loss on lung redox homeostasis in the context of combined *Stk11* loss *in vivo*, making use of the described GEMMs. Using a flow cytometry-based measurement of intracellular ROS (CM-H_2 DCFDA), we observed a doubling of epithelial cells high in ROS levels (defined as $EpCAM^+$CM-H_2 $DCFDA^{high}$) in $Stk11^{fl/fl}Kras^{LSL\text{-}G12D}$ lungs, relatively to $Kras^{LSL\text{-}G12D}$ lungs, that was dramatically decreased upon concurrent *Keap1* loss (Fig. 2F). Assessing lipid peroxidation, a process linked to free oxygen radicals modifying unsaturated fatty acids, revealed a similar pattern: two lipid peroxidation byproducts, thiobarbituric acid-reactive substances (TBARS) and 4-hydroxynonenal (4-HNE), displayed highest levels in $Stk11^{fl/fl}Kras^{LSL\text{-}G12D}$ mouse lungs, whereas concurrent loss of *Keap1* was able to completely reverse the *Stk11*-null phenotype (Fig. 2G–H). *Keap1* loss also significantly increased glutathione (GSH) levels, irrespectively of *Stk11* expression (Fig. 2I). Collectively, these data support the model that *Keap1* loss with ensuing constitutive Nrf2 transcriptional activation - as evidenced through the upregulation of several Nrf2 target genes (Fig. 1B, Fig. S1B) - results in a robust ROS detoxification capacity, neutralizing the increased redox stress induced upon *Stk11* loss *in vivo*.

We confirmed the cooperativity between NRF2 activation and *STK11* loss in maintaining redox balance in human LUAD HCC515 isogenic cell lines with either inducible knockdown of *KEAP1* and/or re-introduction of *STK11* (Fig. S2A–D). Under suspension growth, *STK11*-null HCC515 cells showed decreased viability compared to *STK11*-reconstituted cells and this phenotype was rescued by *KEAP1* knockdown. Accordingly, *KEAP1* knockdown reversed the dramatic increase in ROS levels observed in *STK11*-null cells under suspension conditions (Fig. S2E–F). In the case of *KEAP1* knockdown this phenotype was associated with increased total and *de novo* (M+5, shaded bar) synthesis of the anti-oxidant tripeptide GSH (Fig. S2G). These experiments support the model that *KEAP1* loss, leading to NRF2 activation, can compensate for the loss of *STK11* to maintain low ROS levels via increased total GSH synthesis and enable survival under redox stress conditions.

A transcriptional signature of NRF2 activation is prognostic in primary human lung adenocarcinoma and correlates with low STK11 mRNA expression

We set out to assess the prevalence of functional NRF2 activation, beyond merely genomic alteration, and its clinical impact across human NSCLC. We and others previously released KEAP1/NRF2 signatures (12,20–23). All but one of those signatures were curated from literature or originated from *in vitro* models, with signatures containing genes that associated with *KEAP1* genomic alterations or correlated with known NRF2 targets. Only one *KEAP1*-mutant-specific signature was previously derived from TCGA lung adenocarcinoma tumors; yet, its whole-transcriptome nature limits clinical practicality (11). Herein, we employed a different approach aimed at identifying a core set of *KEAP1/NRF2* associated genes from human tumors that are independent from histology, hence considering both adenocarcinoma and squamous cell carcinoma (7,24), since NRF2 activation is also prevalent in LUSC (35%) (24); further we aimed at identifying genes that were independent from recurrent oncogenic events, namely alterations in *KRAS* and *STK11* in LUAD and *TP53* in LUSC (Fig. 3A, Fig. S3A). As described in Supplementary Materials & Methods, we devised a 96-gene signature of KEAP1/NRF2 pathway activation (Fig. 3B, Fig. S3B–D, Table S2). This signature

Author Manuscript Author Manuscript Author Manuscript Author Manuscript

captures metabolic processes such as glutathione, xenobiotics as well as arachidonic acid metabolism (Fig. 3C, Table S2). A subset of these 96 genes was consistently upregulated in both clinical and pre-clinical NRF2-active tumor samples (Fig. 3D–E, Table S3), and likely represents a set of universal NRF2 targets. Other signature genes were only upregulated in clinical samples, suggesting they may either represent context dependent NRF2 targets in primary human lung cancer and/or features of the tumor microenvironment associated with NRF2 activation, both important to capture in human tumor samples.

By calculating a signature score based on the 96 signature genes and defining histology-specific score thresholds above which a tumor is more likely to have aberrant KEAP1/NRF2 pathway activity, we found that the majority of patients with documented genomic *KEAP1/NRF2* alterations [63% of LUAD and 89% of LUSC] possessed a high signature score (Fig. S3E–F). Reversely, 7% of wild-type LUAD and 24% of wild-type LUSC also had a high signature score (Fig. S3E–F), indicating that a transcriptional signature of NRF2 activation can capture patients displaying functional NRF2 pathway activation in the absence of a documented pathway mutation. Furthermore, our signature was associated more strongly with poor OS in LUAD (multivariate HR = 1.82, p = 0.0011; adjusting for *KRAS* and *STK11* status) (Fig. 3F) than genomic *KEAP1/NRF2* alterations (HR = 1.31, p = 0.14) and remained a poor prognostic factor, even when accounting for genomic *KEAP1/NRF2* alteration status (HR = 2.07, p = 0.0035). While the signature added independent prognostic information beyond genomic *KEAP1/NRF2* alterations (Likelihood Ratio (LR) test, p = 0.0043), the reverse was not true (LR test, p = 0.45). These characteristics were generally true for the various KEAP1/NRF2 signatures, as indicated by a comparative analysis in Fig. S3G–H, Table S4 and S9, and Supplementary Materials & Methods. Finally, in support of a synergistic relationship between concurrent *KEAP1*/*STK11* loss, a high NRF2 activation signature was associated with low *STK11* mRNA expression in primary human LUAD, even among tumors with no documented *STK11* genomic alteration (multivariate model, signature p = 6e-11, *STK11* mutation status p = 0.8, Fig. 3G). Overall, this analysis suggests that a transcriptional signature of NRF2 activation has the potential to be a superior clinical diagnostic tool to *KEAP1/NRF2* mutation status in NSCLC.

NRF2 activation and STK11 mutations associate with shorter survival in docetaxel- and atezolizumab-treated advanced non-squamous lung cancer

To further dissect the impact of NRF2 activation on tumor immune contexture and clinical outcomes, we made use of a clinical lung cancer dataset of second-line (2L+) metastatic or locally advanced NSCLC patient participants in OAK (NCT02008227), a phase III trial comparing standard of care treatment (docetaxel) to the immune checkpoint inhibitor atezolizumab (anti-PD-L1) (25). We first confirmed (i) that the biomarker evaluable populations (BEP) were representative of the intent-to-treat populations (Table S5) and (ii) the robust performance of the NRF2 activation signature in 2L+ non-squamous tumors, including a strong enrichment among *KEAP1/NRF2*-mutant tumors (Fig. 4A, Fig. S4A–B) and a negative association with OS (HR = 1.79, p = 7e-5; Fig. S4C). Importantly, our NRF2 signature captured significant prognostic signal beyond mere genomic *KEAP1/NRF2* alterations (LR test p = 7.8e-4), yet, the reverse was not true (LR test p = 0.77; Table S6). We also confirmed that *STK11*-null tumors were more likely to be NRF2 signature-high

Author Manuscript Author Manuscript Author Manuscript Author Manuscript

(41% of signature-high vs. 13% of signature-low; Fisher's exact test p = 1.8e-7; Fig. 4A; Table S7).

Among patients with *KRAS*-altered tumors, we found that either *STK11* loss and/or NRF2 activation significantly reduced overall survival (Fig. 4B), consistent with our *in vivo* mouse model (Fig. 1A). Yet, a similar negative impact of these two events on overall survival in *KRAS*-wildtype tumors indicated independence from *KRAS* status (Fig. 4C); hence, we further assessed the impact of *STK11* loss and NRF2 activation in the combined sample set, i.e. both *KRAS*-altered and -wildtype tumors.

We found both the NRF2 activation signature and *STK11* mutation status to be prognostic in 2L+ LUAD, irrespectively of treatment arm (NRF2 signature: atezolizumab HR = 1.72, Wald test p = 0.0078; docetaxel HR = 1.98, p = 0.002; *STK11* mutations: atezolizumab HR = 1.54, p = 0.051; docetaxel HR = 2.28, p = 7.3e-5; Fig. 4D–E). In addition, the NRF2 signature and *STK11* mutation status each contributed independently to poor prognosis, across both treatment arms (Fig. S4C–D, see Table S4 for statistics). In contrast, *KRAS* mutation status was not prognostic in either treatment arm (p = 0.76; Fig. 4F, Fig. S4E, Table S6). Instead, while the BEP as a whole trended towards longer survival on atezolizumab compared to docetaxel, *KRAS*-altered tumors were the ones for which this benefit reached statistical significance (HR = 0.53 [CI = 0.35; 0.81], Fig. 4F–G, Table S6). Similar associations with outcome were observed for alternative end points (progression free survival and overall response, Table S6, Fig. S4F–L). Further, observed associations with OS were independent from previously described molecular correlates of response to atezolizumab in NSCLC, PD-L1 protein expression on either immune cells (IC) or tumor cells (TC) as measured by immunohistochemistry (IHC) and tumor mutation burden (26–28) (Supplementary Materials & Methods).

In OAK, patients with high PD-L1 TC expression derived the greatest benefit from atezolizumab, although OS improvement versus docetaxel was noted for the complete range of positive PD-L1 expression (25). Hence, we evaluated PD-L1 protein expression in the context of alterations in *KRAS*, *STK11* and the NRF2 activation signature (Fig. 4H–I). *KRAS* alterations were associated with increased PD-L1 TC staining (LR test p = 2.2e-6, Fig. 4H), which may partially explain the improved survival of patients with *KRAS*-altered tumors when treated with atezolizumab, relative to docetaxel (Fig. 4F–G). In contrast, *STK11* mutations were negatively associated with PD-L1 TC expression, however only in the context of a co-existing *KRAS* alteration: while 3% of *STK11*-mutant compared to 51% of *STK11*-wildtype tumors stained positive for PD-L1 on TCs among *KRAS*-altered tumors (Fisher's exact test p = 7.5e-5), there was no significant difference in TC PD-L1 expression by *STK11* status among *KRAS*-wildtype tumors (16% vs. 27%, Fisher's exact test p = 0.73; Fig. 4H). In the case of PD-L1 IC staining, thought to correlate with IFNγ–induced adaptive immune evasion, there was also a negative association with *STK11* mutations and this was observed irrespectively of *KRAS* status (LR test p = 3.8e-4, Fig. 4I). The NRF2 activation signature was also negatively associated with PD-L1 TC staining, however this was likely driven by the enrichment for *STK11*-mutant tumors among NRF2 signature-high patients. Of note, despite their negative association with PD-L1 expression and negative prognostic outlook, both *STK11*-mutant and NRF2 signature-high tumors

Author Manuscript Author Manuscript Author Manuscript Author Manuscript

derived benefit from atezolizumab to a similar extent as the overall evaluable patient population, irrespectively of *KRAS* status (Fig. 4G).

OAK being an immunotherapy trial, we assessed whether NRF2 activation as well as *KRAS* and *STK11* alterations impacted the tumors' immune contexture. To do so, we calculated scores for established immune cell signatures (Table S8). Expression of a signature estimating infiltration by T effector cells trended towards statistical significance (F-test p = 0.05) for being lowest in the *STK11*-mutant /NRF2 signature-high subgroup (Fig. S4M). The NK cell gene signature, however, showed significantly higher expression among *STK11*-mutant/NRF2 signature-low tumors (Tukey's HSD test p = 0.035) (Fig. S4N). Expression of a dendritic cell (DC) signature was significantly reduced in tumors with high NRF2 signature score, without (p = 0.030) and with concurrent *STK11* mutations (p < 0.001) (Fig. S4O). On the other hand, a myeloid gene expression signature was more highly expressed in *STK11*-mutant only tumors (p = 0.003) (Fig. S4P). Consistent with our mouse models, we observed a positive association of the mucin gene expression signature with *STK11* loss (p <<< 0.001) (Fig. S4Q), and a negative association of NKX2–1 expression with NRF2 activation in the absence of *STK11* loss (p = 0.001) (Fig. S4R).

To summarize, in 2L+ LUAD, we find that high expression of the NRF2 activation signature and *STK11* inactivation are two independent negative prognostic factors, associated with inferior outcomes to both chemotherapy and immunotherapy regimens. In contrast, *KRAS* alterations are associated with a better response to atezolizumab versus docetaxel treatment in this patient population. NRF2 signature score, *STK11* inactivation and *KRAS* alterations have different effects on tumor phenotype and immune contexture, manifested through their distinct impact on PD-L1 immune checkpoint expression on tumor and immune cells, and their association with immune cell gene expression signatures.

Advanced squamous lung cancer patients without NRF2 activation experience longer overall survival when receiving atezolizumab

Finally, we expanded our analyses to OAK participants with squamous tumors (2L+ LUSC), testing the association of our NRF2 activation signature with overall survival, PD-L1 protein expression and impact on tumor immune contexture (Fig. S5A–E, G–I). Strikingly, the NRF2 signature was negatively associated with OS only for patients who received atezolizumab (HR = 1.768 [CI = 1.094; 2.856]), not for those on docetaxel (HR = 1.068 [CI = 0.696; 1.639], Fig. S5C–D). While these data suggest that a low NRF2 signature score may be predictive of benefit from atezolizumab therapy in squamous lung (Fig. S5E), a formal test for the interaction between the NRF2 signature and treatment arm in affecting survival did not reach significance (LR test p = 0.111).

Intrigued by this finding, we validated this association in another independent clinical data set, IMpower131 (NCT02367794) (Fig. 5A, Fig. S5F). IMpower131 is a phase III trial in first line (1L) stage IV squamous NSCLC, comparing the efficacy of a combination of atezolizumab plus chemotherapy (ACP or ACNP) versus chemotherapy alone (CNP; *C*arboplatin + *N*ab-*P*aclitaxel) (29). While 54% of 2L+ patients were NRF2 signature-high (OAK, Fig. S5A–B), only 32% of tumors exhibited NRF2 activation in 1L (IMpower131, Fig. 5A). We confirmed in this 1L LUSC population that NRF2 signature-low patients

Author Manuscript Author Manuscript Author Manuscript Author Manuscript

derived unique survival benefit only when treated with atezolizumab-containing treatment regimens (ACP vs. CNP: HR = 0.754 [CI = 0.595; 0.955]; ACNP vs. CNP: HR = 0.724 [CI = 0.574; 0.913]; Fig. 5B). Still, a formal test for interaction between the NRF2 signature and treatment arm in affecting survival did not reach significance (LR test p = 0.60, comparing CNP to ACNP), possibly due to the large percentage (>50%) of patients in the control arm who received immunotherapy follow-on therapies (29).

All tested immune signatures were significantly more lowly expressed in NRF2 activated, 1L squamous tumors (Fig. 5C). The same associations were apparent in 2L+ LUSC, with the myeloid gene signature reaching significance (adjusted Wilcoxon test p = 0.011) (Fig. S5G). Interestingly, we did not observe an association of the NRF2 activation signature with PD-L1 TC or IC staining in LUSC in either the IMpower131 (Fig. 5D–E) or OAK (Fig. S5H–I) data sets.

We conclude that NRF2 activation impacts the tumor immune contexture in both 1L and 2L+ LUSC. Further, patients with low expression of our NRF2 activation signature show superior survival when treated with atezolizumab, while patients with a NRF2-activated tumor have poor prognosis and remain a high unmet clinical need population.

Discussion

Human lung cancer is a heterogeneous disease (1), hence understanding the impact of key oncogenic drivers on disease biology and clinical outcomes is key for the design of new therapies. Early preclinical studies using GEMMs demonstrated a critical role for NRF2 activation in $Kras^{G12D}$-driven lung tumorigenesis (10), while more recently deletion of *Keap1* either via CRISPR or Cre-loxP recombination technology was found to accelerate $Kras^{G12D}$-induced *in vivo* lung tumorigenesis both alone and in the context of co-deletion with additional tumor suppressors such as *p53* or *PTEN* (10–12,30,31). However, given that in human LUAD, *KEAP1* loss and NRF2 activation often co-occur with the loss of *STK11* in *KRAS*-altered patients, dedicated studies assessing the interplay between these three events are warranted to reveal their epistatic relationships. Prior studies of $Kras^{G12D}Stk11^{-/-}$ lung tumorigenesis found *Stk11* loss to accelerate *Kras*-driven lung tumorigenesis, and described a high degree of tumor heterogeneity and plasticity, attributed to features such as tumor cell-of-origin and redox state (18,32–34). By comparison, targeting the *Keap1* locus in a $Kras^{G12D}Stk11^{fl/fl}$ GEMM using Cre-loxP recombination technology has only recently been reported for a small cohort of mice (12). That study found survival of mice not to be statistically different between $Kras^{G12D}Stk11^{fl/fl}$ and $Kras^{G12D}Stk11^{fl/fl}Keap1^{fl/fl}$ mice, concluding that *Keap1* loss did not cooperate with *Stk11* loss *in vivo* (12). While these data appear to contrast with our findings, likely the number of mice evaluated post-intranasal virus delivery was too small and the survival data too variable to have sufficient statistical power to detect anything other than large survival differences (12,35). Overall, we believe that these differences in experimental design allow us to more accurately model the triple mutant phenotype *in vivo* and interrogate the interplay between *Keap1* and *Stk11* loss in $Kras^{G12D}$-driven lung tumorigenesis.

Author Manuscript Author Manuscript Author Manuscript Author Manuscript

We conclude that *Keap1* loss synergizes with the loss of *Stk11* and the activation of $Kras^{G12D}$ in promoting early-onset, multi-focal tumor initiation, with triple mutant tumors showing an aggressive phenotype of increased proliferation and intra-airway growth, not seen among *Stk11*-null tumors. We propose that these features lead to early lung dysfunction and lethality in $Keap1^{fl/fl}Stk11^{fl/fl}Kras^{LSL\text{-}G12D}$ animals within 6–8 weeks post-infection. Another key observation from our GEMMs is the high prevalence of mucinous hyperplasia and mucinous adenocarcinoma among $Stk11^{fl/fl}Kras^{LSL\text{-}G12D}$ lungs, arising as early as 6–12 weeks pvi and maintained upon concurrent deletion of *Keap1*. At first glance, this may appear to contrast with the high prevalence of adeno-squamous and squamous histologies previously reported among $Stk11^{fl/fl}Kras^{LSL\text{-}G12D}$ tumors (18,32,33). However, our data suggest that there is a kinetic component driving the differentiation state of $Stk11^{fl/fl}Kras^{LSL\text{-}G12D}$ tumors: while squamous carcinomas were rare upon *Stk11* loss or combined *Keap1/Stk11* loss at the early timepoints of 6–12 weeks, prevalence increased at later timepoints (12–19 weeks). Indeed, during the latter interval, $Stk11^{fl/fl}Kras^{LSL\text{-}G12D}$ lungs displayed a high fraction of squamous carcinomas (40%) often co-occurring with regions of adenocarcinoma and mucinous differentiation, consistent with the histological heterogeneity and prevalence previously reported for $Stk11^{fl/fl}Kras^{LSL\text{-}G12D}$ tumors (18). Interestingly, we confirmed a significant, positive association between *STK11* loss and a high mucinous gene expression signature in primary and advanced human LUAD, suggesting that the mouse histology captures characteristics of human tumors. This association occurred irrespectively of NRF2 activation in both human LUAD and our GEMMs, consistent with *STK11* loss being a dominant driver of this differentiation phenotype. The apparent discrepancy in association of mucinous differentiation with *STK11* loss reported herein, versus with low NKX2–1 expression and *CDKN2A/B* loss reported in (8), is caused by differences in genomic-based versus transcriptome-based classification of tumors and the fact that genomic alterations reflect merely an enrichment in, rather than exclusivity to, transcriptional-based subgroups of tumors.

In addition to mouse modeling, we analyzed human clinical datasets to dissect the individual contributions of NRF2 activation, *STK11* loss and *KRAS* alterations to clinical outcomes and phenotypic characteristics of primary and advanced human lung cancer. For this purpose, we utilized clinical and gene expression data from two large cohorts of first-line and second-line NSCLC patients treated with anti-PD-L1 (atezolizumab) and/or chemotherapy (25,29), in addition to the TCGA dataset. We derived a 96-gene NRF2 activation signature valid independently of tumor histology and frequently co-occurring oncogenic alterations. The fact that this and other NRF2 activation signatures (12,20,21) have a higher prognostic power compared to genomic *KEAP1/NRF2* alterations alone (Table S9) suggests that transcriptional profiling captures functional NRF2 activation more broadly and thus has the potential, pending prospective validation, to serve as an improved diagnostic for functional NRF2 pathway deregulation across NSCLC; such a functional signature is hence particularly suited for future therapeutic approaches blocking the NRF2 pathway, contrary to mutant-specific inhibitors. It is intriguing that not all patients harboring genomic alterations in *KEAP/NRF2* exhibit NRF2 pathway activation, as determined by our signature, stressing the necessity, albeit out of scope for this study, of a detailed analysis of the functional consequences of individual mutations. Of note, we did not find an association

Author Manuscript Author Manuscript Author Manuscript Author Manuscript

between NRF2 activation and BACH1, previously shown to be activated under conditions of reduced oxidative stress and to stimulate glycolysis-dependent lung adenocarcinoma metastasis (36,37). Expression of BACH1 and BACH1-dependent genes such as HO-1 as well as redox stress were not associated with *KEAP1/NRF2* alterations, in neither the *in vivo* models and human tumors.

Our NRF2 signature is associated with negative prognosis in both primary (TCGA) and advanced LUAD (OAK). While a previous KEAP1/NRF2 signature has also been associated with worse outcomes in primary LUAD (TCGA) (11), to the best of our knowledge no prior study directly compared the individual impact of NRF2 activation on treatment response to the two standard-of-care regimens (chemotherapy and immunotherapy) in an advanced lung cancer patient cohort (such as the OAK dataset). A prior report presenting data from three patient cohorts without control arms (i.e. single-arm studies) as well as a phase III trial with limited numbers of *KRAS*-mutant, *STK11*-null tumors (n = 6 for anti-PD-1 and n = 3 for docetaxel arms) proposed *STK11* loss to be a genomic driver of resistance to PD-1 checkpoint inhibitors in *KRAS*-mutant lung adenocarcinoma, suggesting it to be predictive rather than prognostic (9). Our 2L+ LUAD dataset has sufficient patient numbers to establish *STK11* loss, like NRF2 activation, as associated with poor overall survival not only in the context of anti-PD-L1 treatment, but also docetaxel treatment. We also took advantage of biomarker IHC data in our 2L+ LUAD cohort to identify a novel, positive association between PD-L1 protein expression on tumor cells and the presence of *KRAS* alterations, consistent with an improved survival of patients with *KRAS*-altered tumors when treated with PD-L1 blockade compared to docetaxel treatment. Conversely, *STK11* mutations were associated with reduced PD-L1 protein expression on immune cells and – only in the context of concurrent *KRAS* alterations – on tumor cells; this finding expands on previous reports that associated *STK11* loss with a lack of PD-L1 expression on tumor cells, irrespective of *KRAS* status (8,9). The requirement for combined *STK11* loss and *KRAS* activation may reflect a distinct epigenetic state of the PD-L1 promoter in those tumors, given that PD-L1 TC expression has been proposed to be regulated via hypermethylation of the PD-L1 promoter (38). Tumor PD-L1 expression may also be linked to tumor differentiation state: for example, mucinous adenocarcinomas have previously been reported to express low PD-L1 levels (17). Unlike TC expression, the association between *STK11* mutations and low PD-L1 IC expression is valid independently of *KRAS* status, likely reflecting an “immune cold” tumor microenvironment (38).

Analysis of two LUSC datasets revealed that our NRF2 signature is not prognostic among both 1L (IMpower131) and 2L+ (OAK) LUSC patients. Instead, we report that LUSC patients with a low NRF2 signature show superior survival when treated with an atezolizumab-containing regimen and not with chemotherapy alone. While these observations are consistent with the lack of association between survival and NRF2 signature expression in LUSC TCGA and hence with an immunotherapy-specific survival benefit, the evolving treatment landscape for NSCLC towards immunotherapy-centric will make a definite assessment of predictive versus prognostic effect of our NRF2 signature challenging – and arguably obsolete. Yet, our findings point towards a potential role for NRF2 in promoting immune evasion in LUSC, especially considering the negative association between the NRF2 signature and all tested immune signatures; these data

Author Manuscript Author Manuscript Author Manuscript Author Manuscript

suggest that NRF2-high tumors are less immune infiltrated and consistent with lack of benefit from immunotherapy for NRF2-high tumors. The fact that these tumors are generally refractory to current treatment options might explain the relative enrichment of NRF2-activated tumors in 2L+ patients (54% vs. 32% in 1L) and further emphasizes the need to develop better therapeutic options for affected patients. Of note in LUSC, NRF2 signature status had no impact on PD-L1 expression on either immune or tumor cells. Overall, our data supports the model that a tumor's genetic make-up directly or indirectly impacts its immune contexture and indicates that better knowledge of this association may help design better future therapies to improve treatment efficacy across NSCLC.

Although current standard of care including chemotherapy and immunotherapy will remain in effect until alternative treatment options have been established, it will be important to either prospectively and/or retrospectively evaluate the status of each oncogenic driver relative to patient outcomes, given that NRF2 status, *STK11* loss or KRAS activation can confer unique tumor response profiles and vulnerabilities. As a diagnostic tool, our or other NRF2 activation signatures have the potential to more accurately identify patients with functional pathway activation beyond *KEAP1* and *NFE2L2* mutational status and help guide future clinical decision-making. Our data also provide further rationale for therapeutic targeting of NRF2 in pathway-activated tumors, an area of high unmet medical need, given their worse outcomes and poor responses to currently available treatments. Our mouse model, showing rapid disease initiation and progression in the context of *Stk11* loss, may be a useful tool for evaluating future NRF2-targeting agents in an *in vivo* setting.

Supplementary Material

Refer to Web version on PubMed Central for supplementary material.

Acknowledgments

We would like to thank Melissa R. Junttila for critical comments on the manuscript and Scott Foster for helpful discussions.

Financial support: Part of this work was supported by grants from the National R&D Program for Cancer Control, Ministry of Health & Welfare, Republic of Korea (1420320, HA17C0033) and the Basic Science Research Program through the National Research Foundation of Korea (NRF) funded by the Ministry of Science, ICT & Future Planning (NRF-2017R1C1B2003162) to S.-M. Jeon. AS was supported by Flight Attendant Medical Research Institute and Maryland Cigarette Restitution Fund. SB is supported with NIH R01CA206155.

References

1. Chen Z, Fillmore CM, Hammerman PS, Kim CF, Wong K-K. Non-small-cell lung cancers: a heterogeneous set of diseases. Nat Rev Cancer. 2014;14:535–46. [PubMed: 25056707]
2. Kensler TW, Wakabayashi N, Biswal S. Cell survival responses to environmental stresses via the Keap1-Nrf2-ARE pathway. Annu Rev Pharmacol Toxicol. 2007;47:89–116. [PubMed: 16968214]
3. Shibata T, Ohta T, Tong KI, Kokubu A, Odogawa R, Tsuta K, et al. Cancer related mutations in NRF2 impair its recognition by Keap1-Cul3 E3 ligase and promote malignancy. Proc Natl Acad Sci U S A. 2008;105:13568–73. [PubMed: 18757741]
4. Singh A, Misra V, Thimmulappa RK, Lee H, Ames S, Hoque MO, et al. Dysfunctional KEAP1-NRF2 interaction in non-small-cell lung cancer. PLoS Med. 2006;3:e420. [PubMed: 17020408]
5. Singh A, Boldin-Adamsky S, Thimmulappa RK, Rath SK, Ashush H, Coulter J, et al. RNAi-mediated silencing of nuclear factor erythroid-2-related factor 2 gene expression in non-small

Author Manuscript Author Manuscript Author Manuscript Author Manuscript

cell lung cancer inhibits tumor growth and increases efficacy of chemotherapy. Cancer Res. 2008;68:7975–84. [PubMed: 18829555]

6. Hast BE, Cloer EW, Goldfarb D, Li H, Siesser PF, Yan F, et al. Cancer-derived mutations in KEAP1 impair NRF2 degradation but not ubiquitination. Cancer Res. 2014;74:808–17. [PubMed: 24322982]
7. The Cancer Genome Atlas Research Network. Comprehensive molecular profiling of lung adenocarcinoma. Nature. 2014;511:543–50. [PubMed: 25079552]
8. Skoulidis F, Byers LA, Diao L, Papadimitrakopoulou VA, Tong P, Izzo J, et al. Co-occurring genomic alterations define major subsets of KRAS-mutant lung adenocarcinoma with distinct biology, immune profiles, and therapeutic vulnerabilities. Cancer Discov. 2015;5:860–77. [PubMed: 26069186]
9. Skoulidis F, Goldberg ME, Greenawalt DM, Hellmann MD, Awad MM, Gainor JF, et al. STK11/LKB1 Mutations and PD-1 Inhibitor Resistance in KRAS-Mutant Lung Adenocarcinoma. Cancer Discov. 2018;8:822–35. [PubMed: 29773717]
10. DeNicola GM, Karreth FA, Humpton TJ, Gopinathan A, Wei C, Frese K, et al. Oncogene-induced Nrf2 transcription promotes ROS detoxification and tumorigenesis. Nature. 2011;475:106–9. [PubMed: 21734707]
11. Romero R, Sayin VI, Davidson SM, Bauer MR, Singh SX, LeBoeuf SE, et al. Keap1 loss promotes Kras-driven lung cancer and results in dependence on glutaminolysis. Nat Med. 2017;23:1362–8. [PubMed: 28967920]
12. Best SA, Ding S, Kersbergen A, Dong X, Song J-Y, Xie Y, et al. Distinct initiating events underpin the immune and metabolic heterogeneity of KRAS-mutant lung adenocarcinoma. Nat Commun. 2019;10:4190. [PubMed: 31519898]
13. Blake DJ, Singh A, Kombairaju P, Malhotra D, Mariani TJ, Tuder RM, et al. Deletion of Keap1 in the lung attenuates acute cigarette smoke-induced oxidative stress and inflammation. Am J Respir Cell Mol Biol. 2010;42:524–36. [PubMed: 19520915]
14. Harvey CJ, Thimmulappa RK, Sethi S, Kong X, Yarmus L, Brown RH, et al. Targeting Nrf2 signaling improves bacterial clearance by alveolar macrophages in patients with COPD and in a mouse model. Sci Transl Med. 2011;3:78ra32.
15. Kong X, Thimmulappa R, Craciun F, Harvey C, Singh A, Kombairaju P, et al. Enhancing Nrf2 pathway by disruption of Keap1 in myeloid leukocytes protects against sepsis. Am J Respir Crit Care Med. 2011;184:928–38. [PubMed: 21799073]
16. Bardeesy N, Sinha M, Hezel AF, Signoretti S, Hathaway NA, Sharpless NE, et al. Loss of the Lkb1 tumour suppressor provokes intestinal polyposis but resistance to transformation. Nature. 2002;419:162–7. [PubMed: 12226664]
17. Guo M, Tomoshige K, Meister M, Muley T, Fukazawa T, Tsuchiya T, et al. Gene signature driving invasive mucinous adenocarcinoma of the lung. EMBO Mol Med. 2017;9:462–81. [PubMed: 28255028]
18. Ji H, Ramsey MR, Hayes DN, Fan C, McNamara K, Kozlowski P, et al. LKB1 modulates lung cancer differentiation and metastasis. Nature. 2007;448:807–10. [PubMed: 17676035]
19. Jeon S-M, Chandel NS, Hay N. AMPK regulates NADPH homeostasis to promote tumour cell survival during energy stress. Nature. 2012;485:661–5. [PubMed: 22660331]
20. DeNicola GM, Chen P-H, Mullarky E, Sudderth JA, Hu Z, Wu D, et al. NRF2 regulates serine biosynthesis in non-small cell lung cancer. Nat Genet. 2015;47:1475–81. [PubMed: 26482881]
21. Goldstein LD, Lee J, Gnad F, Klijn C, Schaub A, Reeder J, et al. Recurrent Loss of NFE2L2 Exon 2 Is a Mechanism for Nrf2 Pathway Activation in Human Cancers. Cell Rep. 2016;16:2605–17. [PubMed: 27568559]
22. Namani A, Cui QQ, Wu Y, Wang H, Wang XJ, Tang X. NRF2-regulated metabolic gene signature as a prognostic biomarker in non-small cell lung cancer. Oncotarget. 2017;8:69847–62. [PubMed: 29050246]
23. Singh A, Boldin-Adamsky S, Thimmulappa RK, Rath SK, Ashush H, Coulter J, et al. RNAi-mediated silencing of nuclear factor erythroid-2-related factor 2 gene expression in non-small cell lung cancer inhibits tumor growth and increases efficacy of chemotherapy. Cancer Res. 2008;68:7975–84. [PubMed: 18829555]

Author Manuscript Author Manuscript Author Manuscript Author Manuscript

24. The Cancer Genome Atlas Research Network. Comprehensive genomic characterization of squamous cell lung cancers. Nature. 2012;489:519–25. [PubMed: 22960745]
25. Rittmeyer A, Barlesi F, Waterkamp D, Park K, Ciardiello F, von Pawel J, et al. Atezolizumab versus docetaxel in patients with previously treated non-small-cell lung cancer (OAK): a phase 3, open-label, multicentre randomised controlled trial. Lancet Lond Engl. 2017;389:255–65.
26. Spigel DR, Chaft JE, Gettinger S, Chao BH, Dirix L, Schmid P, et al. FIR: Efficacy, Safety, and Biomarker Analysis of a Phase II Open-Label Study of Atezolizumab in PD-L1-Selected Patients with Non-Small-Cell Lung Cancer. J Thorac Oncol Off Publ Int Assoc Study Lung Cancer. 2018;
27. Fehrenbacher L, Spira A, Ballinger M, Kowanetz M, Vansteenkiste J, Mazieres J, et al. Atezolizumab versus docetaxel for patients with previously treated non-small-cell lung cancer (POPLAR): a multicentre, open-label, phase 2 randomised controlled trial. Lancet Lond Engl. 2016;387:1837–46.
28. Horn L, Spigel DR, Gettinger SN, Antonia SJ, Gordon MS, Herbst RS, et al. Clinical activity, safety and predictive biomarkers of the engineered antibody MPDL3280A (anti-PDL1) in non-small cell lung cancer (NSCLC): update from a phase Ia study. J Clin Oncol. 2015;33:8029–8029.
29. Jotte R, Cappuzzo F, Vynnychenko I, Stroyakovskiy D, Rodríguez-Abreu D, Hussein M, et al. Atezolizumab in Combination With Carboplatin and Nab-Paclitaxel in Advanced Squamous Non-Small-Cell Lung Cancer (IMpower131): Results From a Randomized Phase III Trial. J Thorac Oncol Off Publ Int Assoc Study Lung Cancer. 2020;
30. Jeong Y, Hoang NT, Lovejoy A, Stehr H, Newman AM, Gentles AJ, et al. Role of KEAP1/NRF2 and TP53 Mutations in Lung Squamous Cell Carcinoma Development and Radiation Resistance. Cancer Discov. 2017;7:86–101. [PubMed: 27663899]
31. Best SA, De Souza DP, Kersbergen A, Policheni AN, Dayalan S, Tull D, et al. Synergy between the KEAP1/NRF2 and PI3K Pathways Drives Non-Small-Cell Lung Cancer with an Altered Immune Microenvironment. Cell Metab. 2018;27:935–943.e4. [PubMed: 29526543]
32. Koyama S, Akbay EA, Li YY, Aref AR, Skoulidis F, Herter-Sprie GS, et al. STK11/LKB1 Deficiency Promotes Neutrophil Recruitment and Proinflammatory Cytokine Production to Suppress T-cell Activity in the Lung Tumor Microenvironment. Cancer Res. 2016;76:999–1008. [PubMed: 26833127]
33. Nagaraj AS, Lahtela J, Hemmes A, Pellinen T, Blom S, Devlin JR, et al. Cell of Origin Links Histotype Spectrum to Immune Microenvironment Diversity in Non-small-Cell Lung Cancer Driven by Mutant Kras and Loss of Lkb1. Cell Rep. 2017;18:673–84. [PubMed: 28099846]
34. Li F, Han X, Li F, Wang R, Wang H, Gao Y, et al. LKB1 Inactivation Elicits a Redox Imbalance to Modulate Non-small Cell Lung Cancer Plasticity and Therapeutic Response. Cancer Cell. 2015;27:698–711. [PubMed: 25936644]
35. DuPage M, Dooley AL, Jacks T. Conditional mouse lung cancer models using adenoviral or lentiviral delivery of Cre recombinase. Nat Protoc. 2009;4:1064–72. [PubMed: 19561589]
36. Wiel C, Le Gal K, Ibrahim MX, Jahangir CA, Kashif M, Yao H, et al. BACH1 Stabilization by Antioxidants Stimulates Lung Cancer Metastasis. Cell. 2019;178:330–345.e22. [PubMed: 31257027]
37. Lignitto L, LeBoeuf SE, Homer H, Jiang S, Askenazi M, Karakousi TR, et al. Nrf2 Activation Promotes Lung Cancer Metastasis by Inhibiting the Degradation of Bach1. Cell. 2019;178:316–329.e18. [PubMed: 31257023]
38. Kowanetz M, Zou W, Gettinger SN, Koeppen H, Kockx M, Schmid P, et al. Differential regulation of PD-L1 expression by immune and tumor cells in NSCLC and the response to treatment with atezolizumab (anti–PD-L1). Proc Natl Acad Sci. 2018;115:E10119–26. [PubMed: 30297397]
39. Johnson L, Mercer K, Greenbaum D, Bronson RT, Crowley D, Tuveson DA, et al. Somatic activation of the K-ras oncogene causes early onset lung cancer in mice. Nature. 2001;410:1111–6. [PubMed: 11323676]
40. Bardeesy N, Sinha M, Hezel AF, Signoretti S, Hathaway NA, Sharpless NE, et al. Loss of the Lkb1 tumour suppressor provokes intestinal polyposis but resistance to transformation. Nature. 2002;419:162–7. [PubMed: 12226664]

Author Manuscript Author Manuscript Author Manuscript Author Manuscript

41. Blake DJ, Singh A, Kombairaju P, Malhotra D, Mariani TJ, Tuder RM, et al. Deletion of Keap1 in the lung attenuates acute cigarette smoke-induced oxidative stress and inflammation. Am J Respir Cell Mol Biol. 2010;42:524–36. [PubMed: 19520915]

42. Singh A, Venkannagari S, Oh KH, Zhang Y-Q, Rohde JM, Liu L, et al. Small Molecule Inhibitor of NRF2 Selectively Intervenes Therapeutic Resistance in KEAP1-Deficient NSCLC Tumors. ACS Chem Biol. 2016;11:3214–25. [PubMed: 27552339]

43. Sudini K, Diette GB, Breysse PN, McCormack MC, Bull D, Biswal S, et al. A Randomized Controlled Trial of the Effect of Broccoli Sprouts on Antioxidant Gene Expression and Airway Inflammation in Asthmatics. J Allergy Clin Immunol Pract. 2016;4:932–40. [PubMed: 27130714]

44. Sussan TE, Sudini K, Talbot CC, Wang X, Wills-Karp M, Burd I, et al. Nrf2 regulates gene-environment interactions in an animal model of intrauterine inflammation: Implications for preterm birth and prematurity. Sci Rep. 2017;7:40194. [PubMed: 28071748]

45. Fallica J, Das S, Horton M, Mitzner W. Application of carbon monoxide diffusing capacity in the mouse lung. J Appl Physiol Bethesda Md 1985. 2011;110:1455–9.

46. Limjunyawong N, Craig JM, Lagassé HAD, Scott AL, Mitzner W. Experimental progressive emphysema in BALB/cJ mice as a model for chronic alveolar destruction in humans. Am J Physiol Lung Cell Mol Physiol. 2015;309:L662–676. [PubMed: 26232300]

47. Krupnick AS, Tidwell VK, Engelbach JA, Alli VV, Nehorai A, You M, et al. Quantitative monitoring of mouse lung tumors by magnetic resonance imaging. Nat Protoc. 2012;7:128–42. [PubMed: 22222788]

48. Tidwell VK, Garbow JR, Krupnick AS, Engelbach JA, Nehorai A. Quantitative analysis of tumor burden in mouse lung via MRI. Magn Reson Med. 2012;67:572–9. [PubMed: 21954021]

49. Choi E-J, Jung B-J, Lee S-H, Yoo H-S, Shin E-A, Ko H-J, et al. A clinical drug library screen identifies clobetasol propionate as an NRF2 inhibitor with potential therapeutic efficacy in KEAP1 mutant lung cancer. Oncogene. 2017;36:5285–95. [PubMed: 28504720]

50. Goldstein LD, Lee J, Gnad F, Klijn C, Schaub A, Reeder J, et al. Recurrent Loss of NFE2L2 Exon 2 Is a Mechanism for Nrf2 Pathway Activation in Human Cancers. Cell Rep. 2016;16:2605–17. [PubMed: 27568559]

Author Manuscript
Author Manuscript
Author Manuscript
Author Manuscript

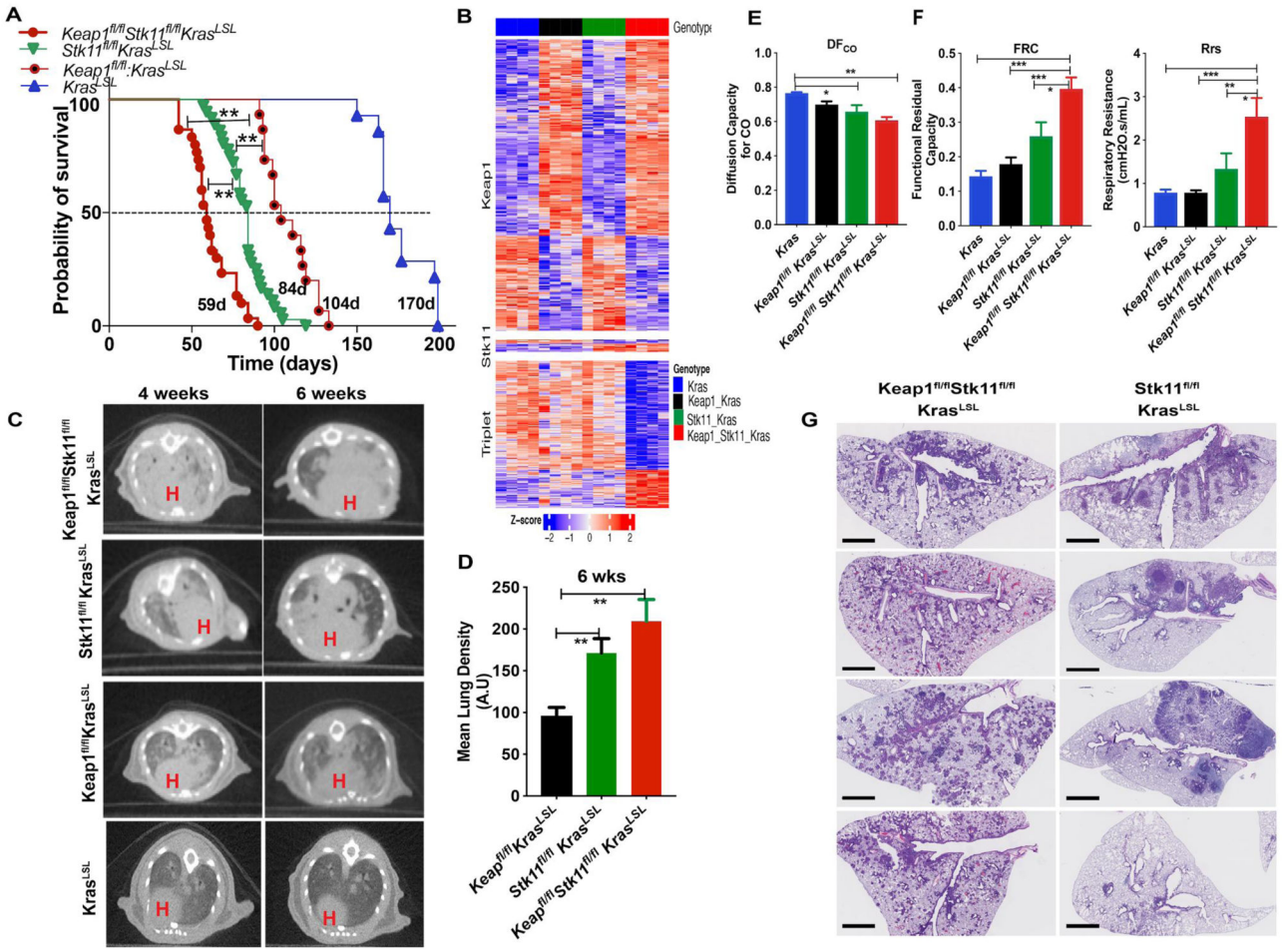

Figure 1. Keap1 inactivation synergizes with Stk11 loss to promote early tumor onset, reduced lung respiratory capacity and mortality in a Kras-driven lung cancer mouse model in vivo

(A) Kaplan Meier Survival plots depicting survival of mice across the different genotypes. 6–8 weeks old animals across each genotype were infected with adenovirus expressing Cre recombinase. Survival curves were generated by pooling animal data from 3–4 experiments. *Keap*$^{fl/fl}$*Stk11*$^{fl/fl}$*Kras*$^{LSL\text{-}G12D}$ (n=30); *Stk11*$^{fl/fl}$*Kras*$^{LSL\text{-}G12D}$ (n=36); *Keap*$^{fl/fl}$*Kras*$^{LSL\text{-}G12D}$ (n=15); *Kras*$^{LSL\text{-}G12D}$ (n=14). **(B)** Expression of 451 genes differentially expressed between *Keap1*-mutant and -wildtype samples, 19 genes differentially expressed between *Stk11*-mutant and -wildtype samples, and 228 genes differentially expressed between the triplet and non-triplet murine lung samples (microarray assessment). Significant differential expression is defined as >2-fold change and adjusted p-value < 0.05. High expression levels are shown in red; low levels in blue. The 16 murine lung samples are annotated by their *Keap1* and *Stk11* status on top of the heatmap. Differentially expressed genes are annotated by the specific comparison on the left of the heatmap. **(C)** CT images of lungs at 4 weeks and 6 weeks post-adenovirus-Cre infection. “H” represents the heart. **(D)** Quantification of lung density from the CT images to estimate lung tumor burden in mice at 6 weeks by ImageJ. CT images from control animals without tumor were used to obtain the baseline lung density values. Eight to ten sections from each mouse were quantified by ImageJ. Of note, several *Keap1*$^{fl/fl}$*Stk11*$^{fl/fl}$*Kras*$^{LSL\text{-}G12D}$ animals had become sick by 6

Author Manuscript Author Manuscript Author Manuscript Author Manuscript

weeks and could not be imaged (n=6–15). **(E-F)** Relative lung function measurements in mice across different genotypes: (**E**) Comparison of diffusion factor for carbon monoxide (DF_{CO}), (**F, left**) functional residual capacity (FRC) and (**F, right**) respiratory system resistance (Rrs) in mice with different genotypes at 6–7 weeks post adeno-Cre infection (n=6). (**G**) Whole lung lobes from $Keap^{fl/fl}Stk11^{fl/fl}Kras^{LSL\text{-}G12D}$ and $Stk11^{fl/fl}Kras^{LSL\text{-}G12D}$ mice to highlight the differences in number and distribution of tumors across the two genotypes. Scale bar corresponds to 2mm. Statistical analysis represents One-way ANOVA : *p<0.05, **p<0.01, ***p<0.001, ****p<0.0001.

Author Manuscript Author Manuscript Author Manuscript Author Manuscript

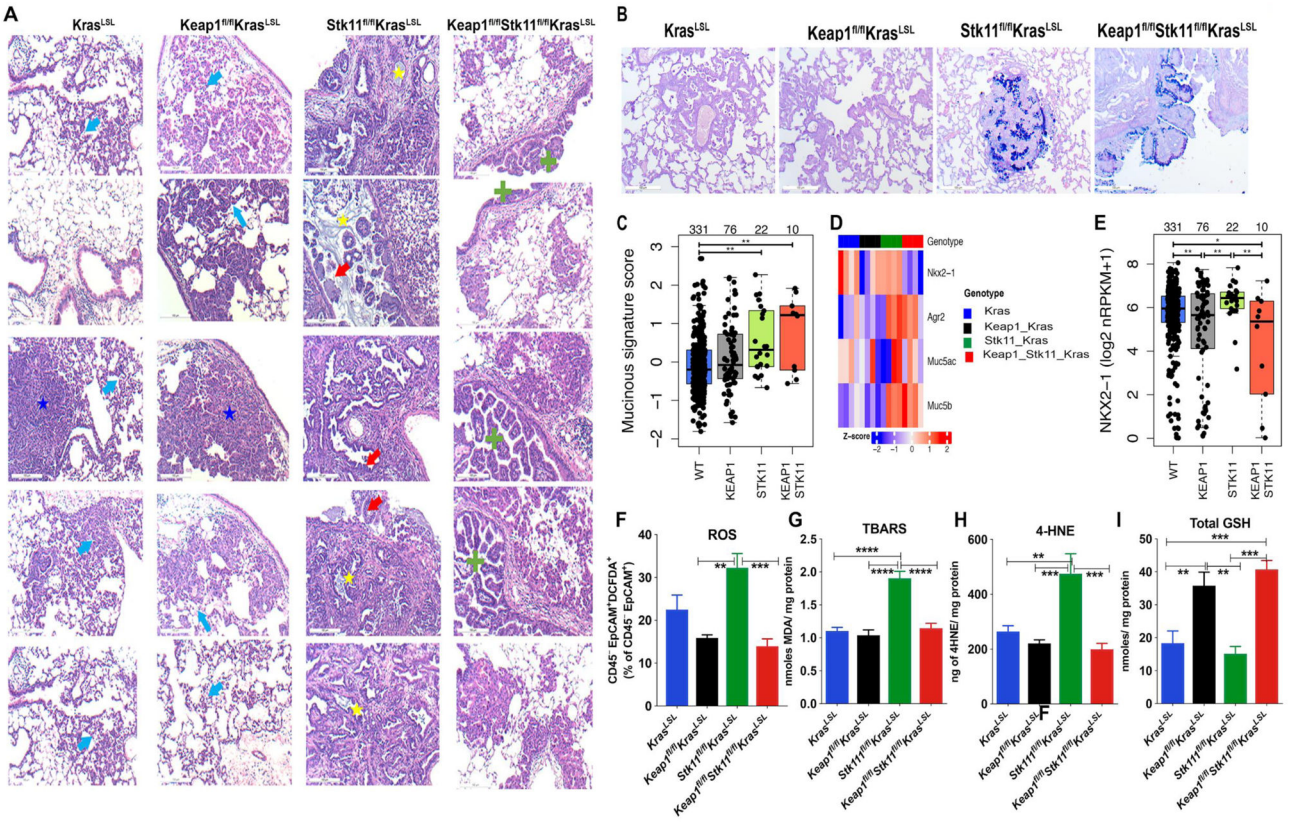

Figure 2. Keap1 loss leads to respiratory distress, associated with an aggressive tumor phenotype, severe airway obstruction, mucinous differentiation, as well as balances redox stress in a Kras-driven lung cancer mouse model with concurrent Stk11 loss

(A) Representative high-magnification images of murine lungs at 7 weeks post adeno-Cre infection for each genotype. Blue Arrow: Atypical adenomatous hyperplasia; Blue Star: Solid adenoma; Red Arrow: Acinar carcinoma with mucous containing neoplastic cells; Yellow Star: Mucous present within gland lumen and airways; Green Cross: Papillary carcinoma. By 6–12 weeks, *Kras*$^{LSL\text{-}G12D}$ mice had only developed coalescing areas of AAH (blue arrow), while *Keap1*$^{fl/fl}$*Kras*$^{LSL\text{-}G12D}$ mice developed more extensive AAH, with a single *Keap1*$^{fl/fl}$*Kras*$^{LSL\text{-}G12D}$ mouse developing an adenoma (blue star) and 4/6 (66%) developing non-mucinous BEH. *Stk11*$^{fl/fl}$*Kras*$^{LSL\text{-}G12D}$ mice showed evidence of mucinous differentiation with large goblet cells (red arrow) and abundant wispy basophilic mucinous material in the alveolar spaces (yellow star). Unique among triple mutant lungs was the presence of intra-bronchiolar papillary carcinomas comprised of a fibrovascular core, long papillary fronds extending into the bronchiole lumen and loaded with abundant viscous mucus. **(B)** Representative images from 6–7-week old *Kras*$^{LSL\text{-}G12}$, *Keap*$^{fl/fl}$*Kras*$^{LSL\text{-}G12D}$, *Stk11*$^{fl/fl}$*Kras*$^{LSL\text{-}G12D}$ and *Keap*$^{fl/fl}$*Stk11*$^{fl/fl}$*Kras*$^{LSL\text{-}G12D}$ lungs stained with Alcian Blue/PAS to assess mucin production. The *Kras*$^{LSL\text{-}G12D}$ and *Keap*$^{fl/fl}$*Kras*$^{LSL\text{-}G12D}$ images display non-mucinous atypical epithelial hyperplasia, the *Stk11*$^{fl/fl}$*Kras*$^{LSL\text{-}G12D}$ image is of a carcinoma with mucinous differentiation and the *Keap*$^{fl/fl}$*Stk11*$^{fl/fl}$*Kras*$^{LSL\text{-}G12D}$ image displays marked bronchiolar epithelial hyperplasia with mucinous differentiation. **(C)** Expression of *Nkx2–1* and mucinous markers in murine lungs. High expression levels are shown in red; low levels in blue. The 16 murine lung

Author Manuscript Author Manuscript Author Manuscript Author Manuscript

samples are annotated by their *Keap1* and *Stk11* status. **(D)** The average expression of mucinous genes *MUC5AC*, *MUC5B* and *AGR2* (mucinous signature score) in function of genotype in TCGA LUAD tumors. Tumors are grouped by *STK11* and/or *KEAP1/NRF2* alteration, independent of *KRAS* status. According to a multivariate linear model of mucinous marker expression as a function of *STK11*, *KEAP1/NRF2*, and *KRAS* status, both *KEAP1/NRF2* and *KRAS* alterations are significantly associated with mucinous marker expression (p = 0.033 and 0.014, respectively), but the effect of *STK11* loss is dominant (p = 5e-5). **(E)** *NKX2–1* expression in function of genotype in TCGA LUAD tumors. Tumors are grouped by *STK11* and/or *KEAP1/NRF2* alteration, independent of *KRAS* status. **(F)** Flow cytometry-based assessment of ROS levels in dissociated mouse lung epithelium tumor cells ($CD45^{-}EpCAM^{+}$) using carboxy-H_2DCFDA dye, graphed as percent of $CD45^{-}EpCAM^{+}$ (n=5). **(G)** Determination of oxidative stress levels in lungs from different genotypes. The TBARS (Thiobarbituric Acid Reactive Substances) assay was used to measure malondialdehyde levels, a marker of lipid peroxidation and resultant oxidative stress (n=7–8). **(H)** 4-hydroxynonenal (4HNE), a common byproduct of lipid peroxidation during oxidative stress, was measured in lung tissue homogenates by ELISA (n=7–8). **(I)** Estimation of total GSH levels in lungs from mice with different genotypes (n=6–8). Statistical analyses represent One-way ANOVA: *p<0.05, **p<0.01, ***p<0.001, ****p<0.0001.

Author Manuscript
Author Manuscript
Author Manuscript
Author Manuscript

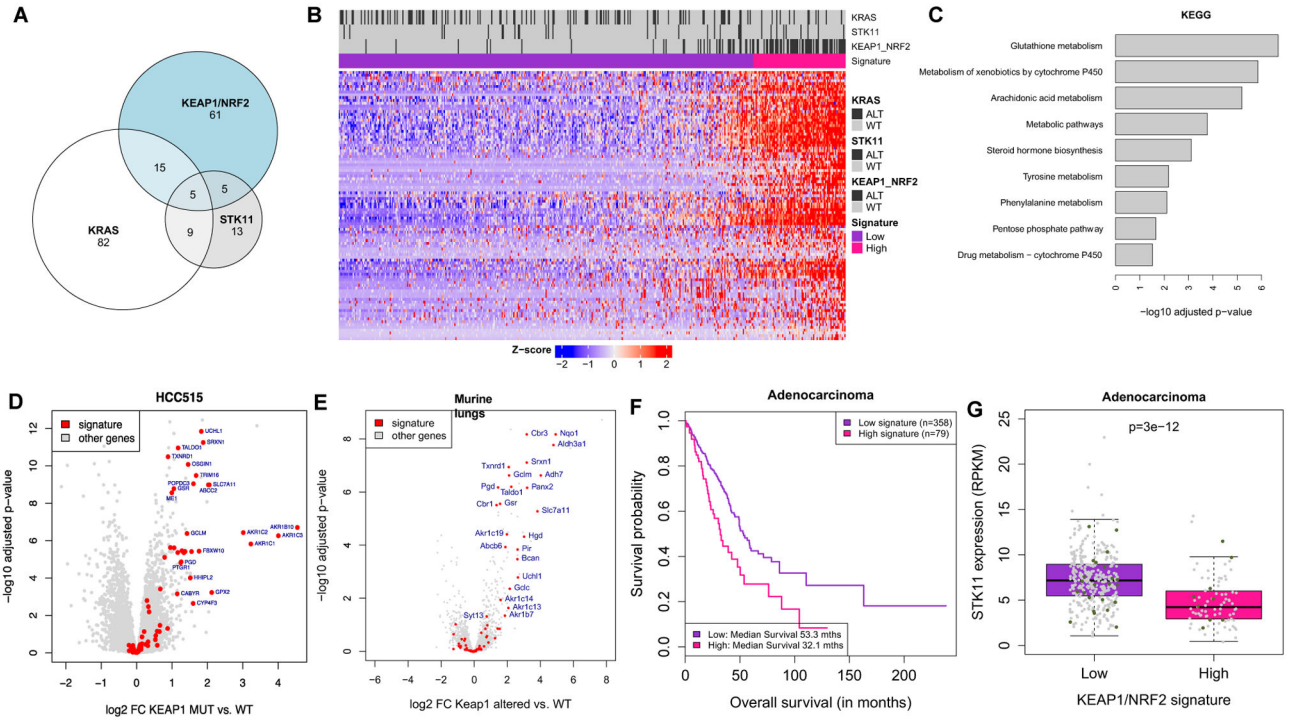

Figure 3. A novel gene expression signature of NRF2 activation is prognostic in primary human lung adenocarcinoma and correlates with low STK11 mRNA expression

(A) Overlap of *KRAS*, *STK11*, and *KEAP1/NRF2* alterations in 439 human lung adenocarcinoma (LUAD) tumors from the TCGA dataset. **(B)** Expression of 96 genes consistently induced by *KEAP1/NRF2* independently of histology, in 439 LUAD tumors. High expression levels are shown in red; low levels in blue. Tumors are annotated by *KRAS*, *STK11*, *KEAP1/NRF2* genomic status, and NRF2 signature score, and ordered by increasing score. **(C)** KEGG pathways significantly enriched within the 96-gene signature, with adjusted p-value <0.05. The full list of KEGG pathways is available in Table S2. **(D)** Volcano plot of genes for the comparison of *KEAP1*-mutant vs. -wildtype HCC515 cells, independent of *STK11* status and media condition. **(E)** Volcano plot of genes for the comparison of *Keap1*-altered vs. -wildtype murine lung samples (independent of *Stk11*). Highlighted in red are 77/96 signature genes with mouse orthologs. **(F)** Kaplan-Meier curve of overall survival (OS) in 428 LUAD patients. High signature is significantly associated with worse OS in a univariate model (HR 1.79, 95% CI 1.25–2.56, p-value 0.0014), and in a multivariate model when accounting for *KRAS* and *STK11* alteration status (HR 1.82, 95% CI 1.27–2.60, p-value 0.0011). **(G)** *STK11* expression by NRF2 signature-low/high in LUAD. *STK11*-mutant tumors are colored in green. Denoted p-value compares NRF2 signature-high vs. low LUAD tumors, using the Mann-Whitney-Wilcoxon test. The association of *STK11* expression with the NRF2 signature is independent of *STK11* mutation status: multivariate linear model predicting *STK11* expression based on signature status and *STK11* status; p-value signature = 6e-11, p-value *STK11* 0.8.

Author Manuscript Author Manuscript Author Manuscript Author Manuscript

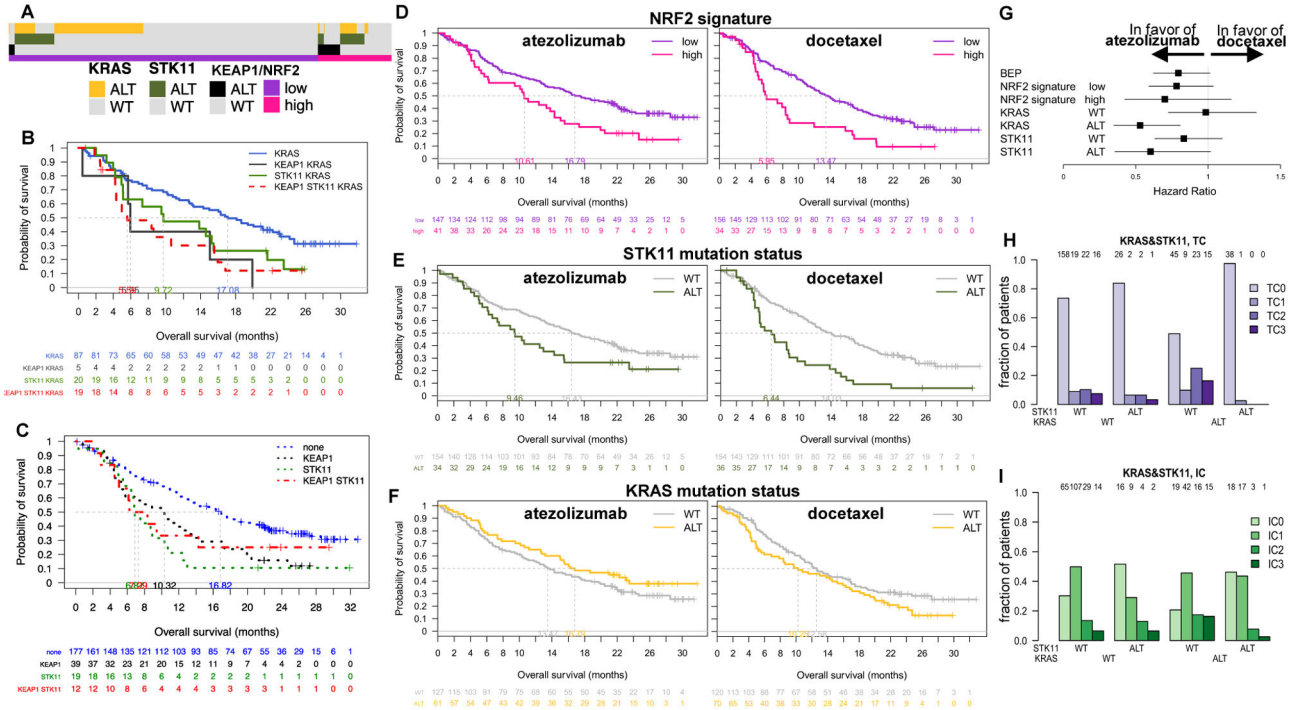

Figure 4. NRF2 activation and STK11 mutations associate with shorter survival in both chemo- and immuno-therapy treated advanced non-squamous lung cancer

(**A**) Visual representation of the relationships between *KEAP1/NRF2* mutations (black), NRF2 activation signature status (purple/pink), *KRAS* (gold) and *STK11* (green) alterations in non-squamous OAK. (**B-C**) Overall survival (OS) of *KRAS*-altered (**B**, n=131) or *KRAS*-wildtype patients (**C**, n=247), depending on NRF2 signature and *STK11* mutation status. Patients lacking *STK11* mutations or NRF2 activation (KRAS, n=87, or none, n=177; blue) have significantly longer survival than patients with either NRF2 activation (KEAP1 KRAS, n=5, or KEAP1, n=39; black), *STK11* mutations (STK11 KRAS, n=20, or STK11, n=19; green) or both (KEAP1 STK11 KRAS, n=19, or KEAP1 STK11, n=12; red) (B: log rank P = 0.006, C: P = 0.0002). **(D-F)** Kaplan Meier curves for overall survival (OS) of 378 non-squamous patients with both transcriptional and mutational profiling, split either by NRF2 signature group **(D)**, by *STK11* mutation status **(E)** or *KRAS* status **(F)**, showing atezolizumab and docetaxel arms separately. Median survival is significantly shorter in the signature score high group in both the atezolizumab (41 patients out of 188; median survival low = 16.8, high = 10.6 months; HR = 1.72; CI = 1.15, 2.58; Wald test p = 0.0078) and docetaxel (34 patients out of 190; median survival low = 13.5, high = 6.0 months; HR = 1.98; CI = 1.31, 3.00; Wald test p = 0.002) arms. Median survival of *STK11*-mutant patients is shorter in the atezolizumab (34 patients out of 188; median survival WT = 16.4, ALT = 9.5 months; HR = 1.54; CI = 0.998, 2.38; Wald test p = 0.051) and docetaxel (36 patients out of 190; median survival WT = 14.0, ALT = 6.4 months; HR = 2.28; CI = 1.52, 3.43; Wald test p = 7.3e-5) arms, although significantly so only in the latter. *KRAS* alterations do not significantly affect survival in either the atezolizumab (61 patients out of 188; median survival WT = 13.5, ALT = 16.8.5 months; HR = 0.75; CI = 0.51, 1.11; Wald test p = 0.15) or the docetaxel arm (70 patients out of 190; median survival WT = 12.6, ALT = 10.3

Author Manuscript Author Manuscript Author Manuscript Author Manuscript

months; HR = 1.39; CI = 0.98, 1.95; Wald test p = 0.061). For a global survival analysis see Fig. S4C–E. (**G**) Forest plot showing the hazard ratios and 95% confidence intervals for different patient subgroups, comparing OS of atezolizumab treated to docetaxel treated patients. **(H-I)** Bar graphs splitting patients by mutation status for *KRAS* and *STK11* (ALT, i.e. altered, or WT, wildtype), showing the fraction of patients in the four categories for PD-L1 protein staining on tumor cells (TC, TC0 <<< TC3, **H**) and immune cells (IC, IC0 <<< IC3, **I**). *KRAS* alterations are associated with higher PD-L1 protein expression on TC (LR test p = 2.2e-6), while *STK11* mutations are associated with lower PD-L1 protein expression on IC (LR test p = 3.8e-4) and, when co-occurring with *KRAS* alterations, on TC (Fisher's exact test p = 7.5e-5). The number of samples per group is indicated above the graph.

Author Manuscript Author Manuscript Author Manuscript Author Manuscript

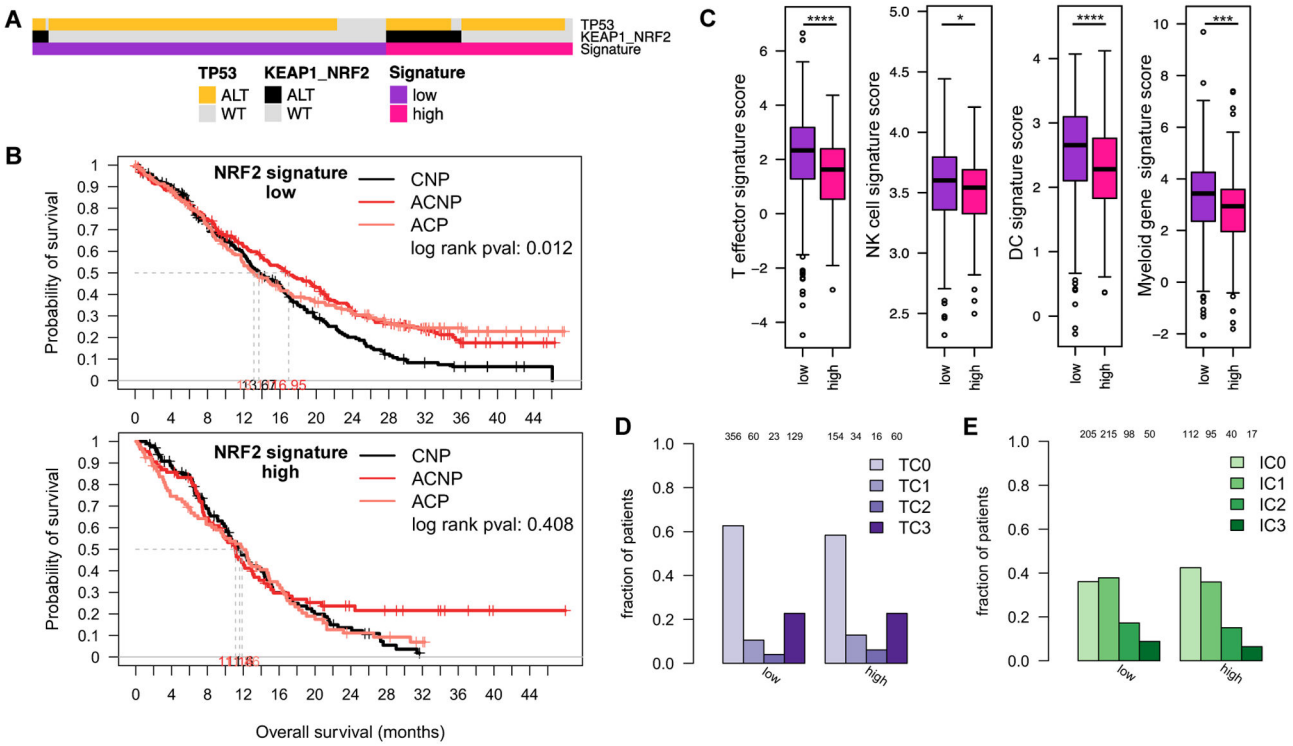

Figure 5. Lack of NRF2 activation associates with longer survival only in immunotherapy, but not chemotherapy treated advanced squamous lung cancer

(**A**) Visual representation of the relationships between *KEAP1/NRF2* mutations (black), NRF2 activation signature status (purple/pink) and *TP53* mutations (gold) in IMpower131. **(B)** Kaplan Meier curves for OS of 832 participants of the IMpower131 trial with transcriptional profiling, split into NRF2 signature-low (top panel, n=568) and high (bottom panel, n=264), comparing the three different treatment arms [arm A: ACP – atezolizumab + carboplatin + paclitaxel (low n=186, high n=80), arm B: ACNP – atezolizumab + carboplatin + nab-paclitaxel (low n=195, high n=84), arm C: carboplatin + nab-paclitaxel (low n=187, high n=100)]. There is a significant difference in survival between arms in NRF2 signature-low (log rank p = 0.012), but not high (p = 0.408) patients. Median survival in months: low ACP = 13.1, ACNP = 17, CNP = 13.7; high ACP = 11.9, ACNP = 11.1, CNP = 11.6. (**C**) Association between T effector, natural killer cell (NK), dendritic cell (DC) and myeloid gene signature expression and NRF2 pathway activation in IMpower131. Gene signature scores are plotted, splitting tumors based on NRF2 activation signature expression ("low", n=568; "high", n=264). Significant differences between groups are observed for all immune signatures (adjusted Wilcoxon p for T effector: 9.80e-9, NK: 0.025, DC: 2.04e-7, myeloid: 5.64e-4). *p<0.05, ***p<0.001, ****p<0.0001. **(D-E)** Bar graphs splitting patients by mutation status for NRF2 activation gene signature status, showing the fraction of patients in the four categories for PD-L1 protein staining on tumor cells (TC, TC0 <<< TC3, **D**) and immune cells (IC, IC0 <<< IC3, **E**). NRF2 pathway activation is neither associated with PD-L1 staining on TC (Fisher's exact test p = 0.38) nor on IC (p = 0.30). The number of samples per group is indicated above the graph.

Author Manuscript

Author Manuscript

Author Manuscript

Author Manuscript

Table 1:

Summary of lung tumor histology assessment across mice with different genotypes, corresponding to Fig 2A. wks: weeks, AAH: atypical adenomatous hyperplasia, AdCA: adenocarcinoma, BEH: bronchiolar epithelial hyperplasia.

Genotype	Age (wks)	AAH	Adenoma	AdCA	Squamous histology	Mucinous histology	Non-Mucinous BEH	Mucinous BEH
Kras ^{LSL}	6–12	4/7	2/7	0/7	0/7	0/7	0/7	0/7
Keap1 $^{fl/fl}$***Kras*** ^{LSL}	6–12	6/6	1/6	0/6	0/6	0/6	4/6	0/6
Stk11 $^{fl/fl}$***Kras*** ^{LSL}	6–12	13/13	8/13	4/13	0/13	12/13	11/13	13/13
Keap1 $^{fl/fl}$***Stk11*** $^{fl/fl}$***Kras*** ^{LSL}	6–12	26/26	17/26	14/26	2/26	6/26	26/26	26/26
Kras ^{LSL}	12–19	3/3	2/3	2/3	0/3	0/3	2/3	0/3
Keap1 $^{fl/fl}$***Kras*** ^{LSL}	12–19	6/6	5/6	2/6	0/6	0/6	5/6	1/6
Stk11 $^{fl/fl}$***Kras*** ^{LSL}	12–19	5/5	3/5	3/5	2/5	3/5	4/5	5/5
Kras ^{LSL}	19–24	6/6	6/6	4/6	0/6	0/6	6/6	0/6